

10-22-2009

Topology optimization of muffler internal partitions for improving acoustical attenuation performance

Jin Woo Lee

Purdue University - Main Campus

Yoon Young Kim

Seoul Natl Univ

Follow this and additional works at: <http://docs.lib.purdue.edu/nanopub>



Part of the [Engineering Commons](#)

Lee, Jin Woo and Kim, Yoon Young, "Topology optimization of muffler internal partitions for improving acoustical attenuation performance" (2009). *Birck and NCN Publications*. Paper 581.

<http://docs.lib.purdue.edu/nanopub/581>

This document has been made available through Purdue e-Pubs, a service of the Purdue University Libraries. Please contact epubs@purdue.edu for additional information.

Topology optimization of muffler internal partitions for improving acoustical attenuation performance

Jin Woo Lee¹ and Yoon Young Kim^{2,*},[†]

¹*Birck Nanotechnology Center, School of Mechanical Engineering, Purdue University, West Lafayette, IN 47907, U.S.A.*

²*National Creative Research Initiatives Center for Multiscale Design, School of Mechanical and Aerospace Engineering, Seoul National University, Seoul 151-742, Republic of Korea*

SUMMARY

The internal partition configuration of an expansion chamber muffler affects significantly its acoustical transmission characteristics, but the use of systematic optimization methods to muffler design problems is rare. The main objective of this research is to maximize the transmission loss at target frequencies by optimizing partition layouts inside a muffler chamber by formulating an acoustical topology optimization problem. The selected target frequencies include the deep frequencies of a nominal muffler in order to see the critical effects of partition configurations on the acoustical transmission characteristics. The effects of partition volume constraint ratios are also investigated and physics behind the optimized layouts is investigated. Numerical results show that mufflers with optimized partition layouts outperform nominal mufflers considerably, but the shapes and locations of the optimized partitions should be much different from those of conventional partitions. Copyright © 2009 John Wiley & Sons, Ltd.

Received 15 September 2008; Revised 5 April 2009; Accepted 8 April 2009

KEY WORDS: muffler design; transmission loss; topology optimization; partition; target frequency; acoustical attenuation performance

1. INTRODUCTION

The optimal design of the internal configuration or geometry of an expansion chamber muffler is important in reducing noise levels in mechanical systems such as ducts, pipes and compressors. Selamat and Radavich [1] studied the length effect of the expansion chamber on acoustical behavior of a muffler. Åbom [2] considered higher-order mode effects to evaluate the acoustical performance

*Correspondence to: Yoon Young Kim, National Creative Research Initiatives Center for Multiscale Design, School of Mechanical and Aerospace Engineering, Seoul National University, San56-1 Shinlim-9-dong, Kwanak-gu, Seoul 151-742, Republic of Korea.

[†]E-mail: yykim@snu.ac.kr

Contract/grant sponsor: National Creative Research Initiatives Program (Korea Science and Technology Foundation); contract/grant numbers: 2007-019, 0420-2008-0011

of an expansion chamber muffler with an extended inlet and outlet. The acoustical attenuation performances of a circular expansion chamber muffler with an extended inlet and outlet and a circular dual-chamber muffler were also studied by Selamet *et al.* [3, 4]. Panigrahi and Munjal [5] developed a generalized algorithm to investigate sound attenuation of complex, multiply connected mufflers. Selamet and Ji [6] investigated the effect of the length-to-diameter ratio of the chamber and the relative locations of the inlet/outlet on the acoustical attenuation performance of circular flow-reversing chamber mufflers. However, these investigations did not use systematic optimization algorithms.

Recently, a shape optimization method was employed for muffler design. For instance, Yeh *et al.* [7] presented a genetic algorithm for the optimal shape design of single-chamber and double-chamber mufflers. Chang and Chiu [8] applied a simulated annealing method to shape optimization of one-chamber perforated plug/non-plug mufflers. Chang *et al.* [9] optimized the shape of double-layer absorbers on constrained sound absorption system. Seo and Kim [10] optimized the arrangement of resonators to increase the peak of the transmission loss (TL) and expand the bandwidth. Barbieri and Barbieri [11] determined the optimal lengths of extended inlets and outlets. Although a topology optimization method can be also effective in muffler design problems, no application has been reported so far. In this work, the muffler design problem is formulated as an acoustical topology optimization problem. The objective is to maximize the TL of a concentric expansion chamber muffler at a target frequency. Note that not only the formulation procedure itself, but also the physical interpretation of optimized results is important for practical applications. In this respect, the main contributions of this investigation are two-fold: the formulation of the muffler design problem as an acoustical topology optimization problem and the physical interpretation of the optimized results.

For acoustical topology optimization formulation, one can use existing approaches such as those developed and used by Lee *et al.* [12], Wadbro and Berggren [13] and Dühring *et al.* [14]. A gradient-based topology optimization scheme and finite element method will be used in this muffler design problem. Thus, the expansion chamber of a muffler will be discretized by acoustical finite elements and one design variable is assigned to each element for controlling the material properties of the element. The material properties are assumed to vary continuously from those of air to those of a rigid body. No flow analysis will be considered in this work. The objective function of the optimization problem is the TL of a muffler at a target frequency. The design constraint on allowed partition volume is given by the maximum number of allowed rigid body elements. The TL value will be evaluated by the three-point method (Wu and Wan [15]). A gradient-based optimization algorithm, called the method of moving asymptotes [16], is used to update design variables. After solving the formulated acoustical topology optimization problem for various target frequencies and numbers of allowed rigid body elements, the optimized results are examined from the viewpoint of muffler acoustics.

2. FUNDAMENTALS OF AN EXPANSION CHAMBER MUFFLER

Figure 1(a) shows a typical expansion chamber muffler having a concentric expansion chamber with an end inlet and an end outlet. To facilitate numerical analysis and optimization, however, the computations will be done in two dimensions with planar symmetry throughout this investigation. The acoustic pressure p inside the expansion chamber muffler is governed by the following

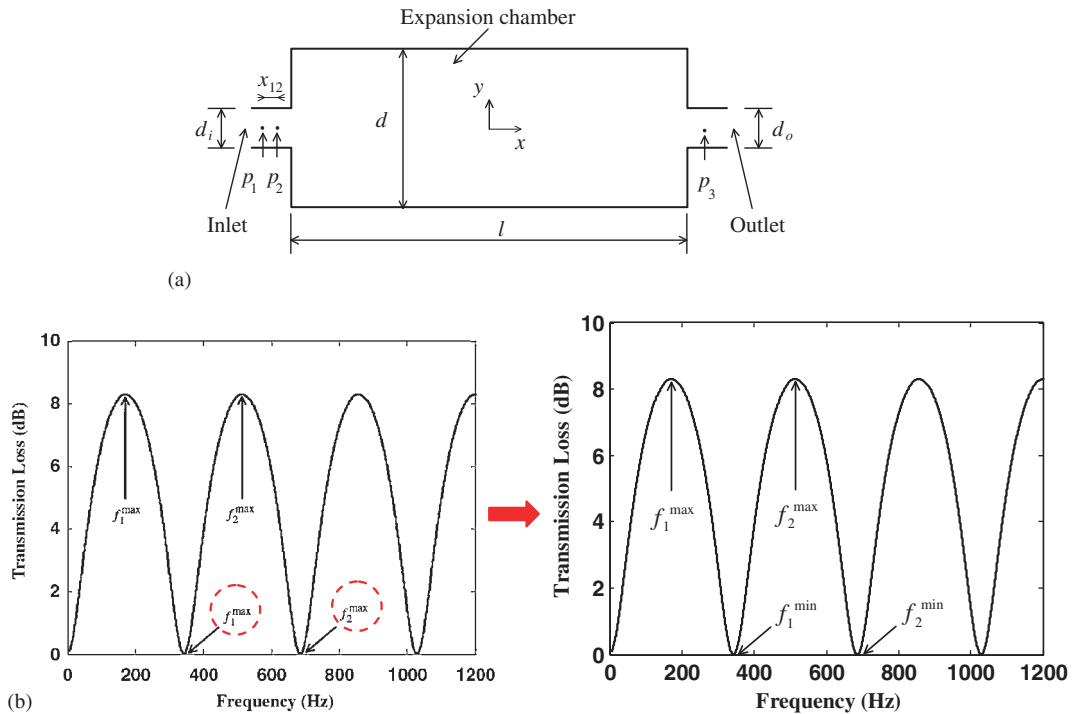


Figure 1. A two-dimensional concentric expansion chamber muffler: (a) geometry and (b) transmission loss curve.

Helmholtz equation [17]:

$$\nabla \cdot \left(\frac{1}{\rho} \nabla p \right) + \frac{\omega^2}{K} \cdot p = 0 \tag{1}$$

The symbol ρ denotes the density, $K = \rho c^2$, the bulk modulus, c , the sound velocity of the acoustic medium, and ω , the angular frequency. The TL values are calculated by using the classical TL formula based on the plane wave theory for a simple expansion chamber muffler [1]

$$TL = 10 \times \log_{10} \left(1 + \frac{1}{4} \left(m - \frac{1}{m} \right)^2 \cdot \sin^2(k \cdot l) \right) \tag{2a}$$

with

$$m = d/d_i, \quad k = 2\pi f/c \tag{2b}$$

where k and f are the wave number and frequency, respectively. The symbols d and d_i denote heights of the two-dimensional expansion chamber and the inlet, respectively. The symbol l is the

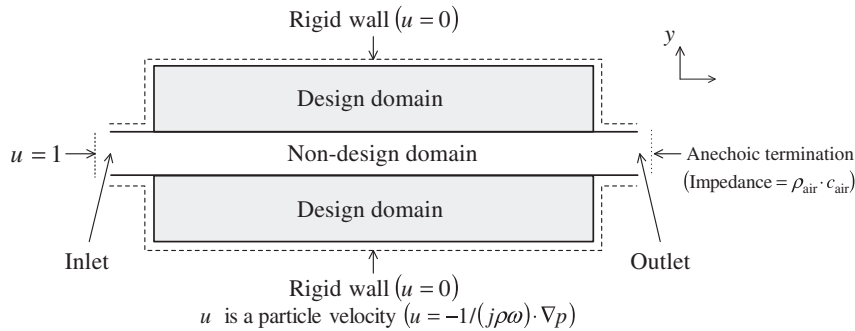


Figure 2. Design domain inside the expansion chamber of a muffler for topology optimization and boundary conditions imposed to each side for finite element analysis.

length of the expansion chamber. The expansion ratio m is the height ratio between an expansion chamber and an inlet (=an outlet) in a two-dimensional expansion chamber muffler: $m = d/d_i$.

For $l = 0.5$ m, $d = 0.15$ m, $d_i = d_o = 0.03$ m and $c = 343$ m/s, the TL in a low-frequency range (less than c/d) is plotted as a function of frequency f in Figure 1(b). It shows that the TL curve exhibits the repetitive dome-like behavior. While the magnitude of TL at $f_i^{\max}(i = 1, \dots)$ increases with the expansion ratio $m(=d/d_i)$, the magnitude of TL at $f_i^{\min}(i = 1, \dots)$ does not change and is almost zero. (This is because f_i^{\min} , known as deep frequencies, closely coincide with the eigenfrequencies of the x -axial acoustic modes of an expansion chamber muffler [6, 18, 19].) Therefore, a simple expansion chamber muffler cannot reduce noise effectively when the frequency range of interest includes deep frequencies or when the magnitude of noise at f_i^{\max} is much larger than the magnitude of TL at f_i^{\max} . An effective way to resolve this shortcoming is to insert partitions inside the expansion chamber of the muffler because partitions can change the acoustical modal properties of a muffler.

For optimal partition distribution in the design domain illustrated in Figure 2, the muffler design problem will be formulated as an acoustical topology optimization problem. The non-design domain is introduced to ensure fluid passage from the inlet to the outlet. Fluid is assumed to be air.

When a partition appears in the design domain of Figure 2, the TL formula in Equation (2) cannot be directly used. Therefore, the three-point method suggested by Wu and Wan [15] will be used to calculate the TL

$$TL = 20 \times \log_{10} \left| \frac{1}{p_3} \frac{p_1 - p_2 \cdot e^{-jk \cdot x_{12}}}{1 - e^{-j2k \cdot x_{12}}} \right|, \quad j = \sqrt{-1} \quad (3)$$

where p_1 , p_2 and p_3 are the acoustic pressures at three points marked in Figure 1(a). In deriving Equation (3), the acoustic pressure is assumed to be time harmonic as $e^{j\omega t}$ (t : time). The distance between two measurement points of the inlet is denoted by x_{12} .

Because the topology optimization requires the acoustical analysis of an expansion chamber muffler, the standard finite element method is used. The finite element approximation of Equation (1) is

$$[\mathbf{K} - \omega^2 \mathbf{M}] \mathbf{P} = \mathbf{F} \quad (4)$$

where \mathbf{P} and \mathbf{F} are the nodal vectors of the acoustic pressure and applied (equivalent) force. The stiffness matrix \mathbf{K} and the mass matrix \mathbf{M} are assembled as

$$\mathbf{K} = \mathbf{A} \sum_{n=1}^N \mathbf{k}_n \tag{5a}$$

$$\mathbf{M} = \mathbf{A} \sum_{n=1}^N \mathbf{m}_n \tag{5b}$$

where $\mathbf{A} \sum_{n=1}^N$ stands for the finite element assembly operator and N is the number of total finite elements in the muffler. The element stiffness matrix \mathbf{k}_n and the element mass matrix \mathbf{m}_n of the n th element are expressed as

$$\mathbf{k}_n = \int_{\Omega_n} \frac{1}{\rho_n} \nabla \mathbf{N}_n^T \nabla \mathbf{N}_n \, d\Omega \tag{6a}$$

$$\mathbf{m}_n = \int_{\Omega_n} \frac{1}{K_n} \mathbf{N}_n^T \mathbf{N}_n \, d\Omega \tag{6b}$$

where \mathbf{N}_n denotes the shape function vector of the n th element. Once the nodal vector \mathbf{P} is calculated by Equation (4), the acoustic pressures p_1, p_2 and p_3 for the TL calculation can be calculated as

$$p_i = \mathbf{L}_i^T \mathbf{P} \quad (i = 1, 2, 3) \tag{7}$$

where \mathbf{L}_i is the vector having the same size as the nodal vector \mathbf{P} and unit magnitude at measurement location i .

The expansion chamber including the design and non-design domains is discretized by 1500 four-node elements. The nodes in the expansion chamber are distributed at uniform spacing of 0.01 m along the x -direction and at uniform spacing of 0.005 m along the y -direction. For finite element calculation, all boundaries except the inlet and the outlet are assumed to be surrounded by rigid walls where the particle velocity is zero. A particle velocity of unit magnitude is imposed at the face of the inlet section, whereas the characteristic impedance of air is imposed at the outlet to simulate anechoic termination [19] (see Figure 2). To implement these two boundary conditions in finite element formulation, the applied equivalent force \mathbf{F} is specified as follows:

$$\mathbf{F} = -j\omega \int_{\partial\Omega_n} \mathbf{N}_n \, d(\partial\Omega) \tag{8}$$

The element mass matrix \mathbf{m}_n in Equation (6b) is replaced by the following expression for the elements with the anechoic termination:

$$\mathbf{m}_n = \int_{\Omega_n} \frac{1}{K_n} \mathbf{N}_n^T \mathbf{N}_n \, d\Omega + \frac{1}{j\omega} \int_{\partial\Omega_n} \frac{1}{\rho_{\text{air}} c_{\text{air}}} \mathbf{N}_n^T \mathbf{N}_n \, d(\partial\Omega) \tag{9}$$

3. TOPOLOGY OPTIMIZATION FORMULATION

In this section, an acoustical topology optimization problem for muffler design will be formulated. Though acoustical topology optimization procedures for other problems are available, a specific formulation suitable for the present muffler design problem will be given.

In this work, the main objective is to maximize the TL value at target frequencies for a constraint on the total number of rigid body elements forming partitions. In this case, the objective function L of the present optimization problem may be selected as

$$\min_{0 \leq \chi_r \leq 1} L = - \sum_{t=1}^T w_t \cdot \text{TL}(f_t) \quad (10)$$

subject to

$$\sum_{r=1}^R \chi_r / R \leq V_a (= R_a / R) \quad (11)$$

The symbol χ_r ($0 \leq \chi_r \leq 1$) is the design variable assigned to the r th finite element of the design domain. When χ_r becomes 0, the element is filled with air and incident acoustic waves can be transmitted to the other side. On the contrary, it simulates a rigid body element fully reflecting incident acoustic waves when χ_r becomes 1. The number of the total finite elements and that of allowed rigid body elements in the design domain are denoted by R and R_a , respectively. Since the rigid body elements form partitions, the ratio of R_a to R is equal to the volume ratio V_a of partitions to the design domain. The symbol w_t is a weighting factor of TL at each target frequency when multiple target frequencies are considered.

The acoustic medium in the non-design domain shown in Figure 2 is air. The finite elements discretizing the design domain are assumed to have real-valued variable acoustical properties, which are the functions of a design variable. In this problem, densities ρ_r and bulk moduli K_r ($r = 1, \dots, R$) of the finite elements are interpolated as

$$1/\rho_r(\chi_r) = 1/\rho_{\text{air}} + \chi_r^\alpha (1/\rho_{\text{rigid}} - 1/\rho_{\text{air}}) \quad (12)$$

$$1/K_r(\chi_r) = 1/K_{\text{air}} + \chi_r^\alpha (1/K_{\text{rigid}} - 1/K_{\text{air}}) \quad (13)$$

where the subscripts 'air' and 'rigid' stand for air and a rigid body, respectively. The exponent α of the design variable is the penalization parameter. (The value of $\alpha = 1$ is used in this investigation.)

The interpolation functions are not unique. In the present TL maximization problem, however, the interpolation function should make the TL with intermediate design variables inferior to the TL with distinct 0–1 design variables for the same volume ratio of partitions to the design domain. Otherwise, distinct 0–1 states of the design variables cannot be obtained at the end of optimization.

To check if the interpolation functional form of Equations (12) and (13) satisfies this criterion, a test problem shown in Figure 3(a) is devised. For numerical calculations, the following data are used:

$$\begin{aligned} d &= 0.2 \text{ m}, & d_i &= 0.1 \text{ m}, & l &= 0.5 \text{ m} \\ R &= 40, & \chi_r &= 0 \quad (r = 1, \dots, 40, \quad r \neq 10, \quad r \neq 30) \\ R_a &= 1, & \chi_{10} + \chi_{30} &= 1, & 0 \leq \chi_{10} \leq 1, & 0 \leq \chi_{30} \leq 1 \\ \rho_{\text{air}} &= 1.21 \text{ kg/m}^3, & c_{\text{air}} &= 343 \text{ m/s}, & K_{\text{air}} &= \rho_{\text{air}} \cdot c_{\text{air}}^2 \\ \rho_{\text{rigid}} &= 10^7 \cdot \rho_{\text{air}}, & K_{\text{rigid}} &= 10^9 \cdot K_{\text{air}} \end{aligned}$$

Note that the total volume of the rigid body elements is fixed due to the constraint $\chi_{10} + \chi_{30} = 1$. For instance, $\chi_{30} = 1$ for $\chi_{10} = 0$, $\chi_{30} = 0.5$ for $\chi_{10} = 0.5$ and $\chi_{30} = 0$ for $\chi_{10} = 1$. Figure 3(b) shows

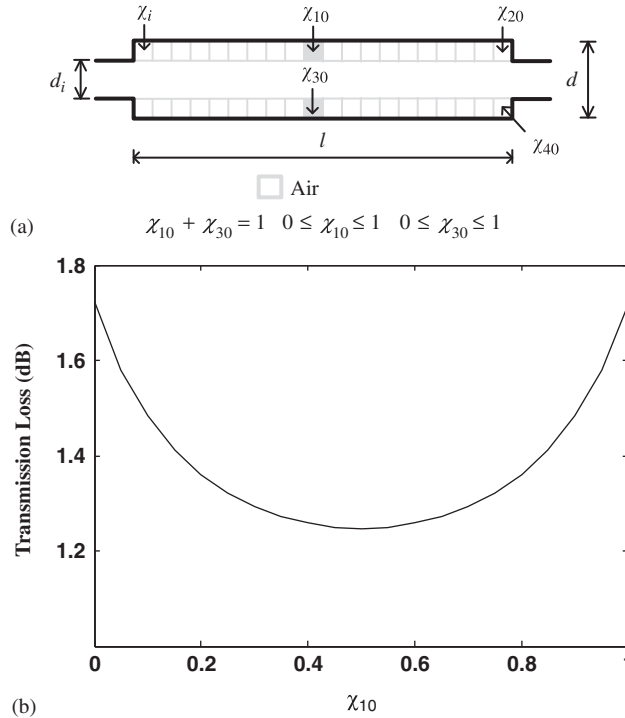


Figure 3. Test problem to check the validity of the interpolation functions given by Equations (12) and (13): (a) a design variable distribution used to test the interpolation functions and (b) variation of TL at 500 Hz by Equations (12) and (13) for $\alpha = 1$.

the values of the TL at 500 Hz as a function of χ_{10} . The TL value reaches the maximum near ($\chi_{30} = 1, \chi_{10} = 0$) or ($\chi_{30} = 0, \chi_{10} = 1$), while it reaches the minimum around $\chi_{10} = 0.5$ and $\chi_{30} = 0.5$. From Figure 3(b), one can see that the interpolation functions of Equations (12) and (13) can favor the distinct 0–1 states of the design variables over intermediate states of the design variables. Therefore, the use of the interpolation functions in Equations (12) and (13) can be effective in obtaining 0–1 states of the design variables at the end of optimization iterations.

To solve the topology optimization problem stated as Equations (10)–(13), the method of moving asymptotes [16], a gradient-based optimizer, is used. The sensitivity $\partial TL(f_t) / \partial \chi_e$ necessary for the optimizer can be calculated by the following analysis:

$$TL(f_t) = 10 \times \log_{10} \frac{|p_{in}|^2}{|p_{out}|^2} \tag{14a}$$

$$|p_{in}| = |(p_1 - p_2 \cdot e^{-jk \cdot x_{12}}) / (1 - e^{-j2k \cdot x_{12}})| \tag{14b}$$

$$|p_{out}| = |p_3| \tag{14c}$$

$$\frac{\partial TL(f_t)}{\partial \chi_r} = \frac{10}{\ln 10} \times \left(\frac{1}{|p_{in}|^2} \cdot \frac{\partial |p_{in}|^2}{\partial \chi_r} - \frac{1}{|p_{out}|^2} \cdot \frac{\partial |p_{out}|^2}{\partial \chi_r} \right) \tag{15}$$

$$|p_{\text{in}}|^2 = \frac{1}{\gamma} (\text{Re}(p_1) - \text{Re}(p_2) \cdot \cos(k \cdot x_{12}) - \text{Im}(p_2) \cdot \sin(k \cdot x_{12}))^2 + \frac{1}{\gamma} (\text{Im}(p_1) - \text{Im}(p_2) \cdot \cos(k \cdot x_{12}) + \text{Re}(p_2) \cdot \sin(k \cdot x_{12}))^2 \quad (16a)$$

$$|p_{\text{out}}|^2 = (\text{Re}(p_3))^2 + (\text{Im}(p_3))^2 \quad (16b)$$

$$\gamma = (1 - \cos(2k \cdot x_{12}))^2 + (\sin(2k \cdot x_{12}))^2 \quad (16c)$$

where $\text{Re}(p_i)$ and $\text{Im}(p_i)$ are the real part and the imaginary part of the acoustic pressure p_i , respectively. The symbol 'ln' in Equation (15) denotes the natural logarithm. The differentiations of the acoustic pressure at three points with respect to each design variable χ_r are as follows:

$$\frac{\partial \mathbf{P}}{\partial \chi_r} = -[\mathbf{K} - \omega^2 \mathbf{M}]^{-1} \left[\frac{\partial \mathbf{K}}{\partial \chi_r} - \omega^2 \frac{\partial \mathbf{M}}{\partial \chi_r} \right] \mathbf{P}, \quad \omega = 2\pi f \quad (17)$$

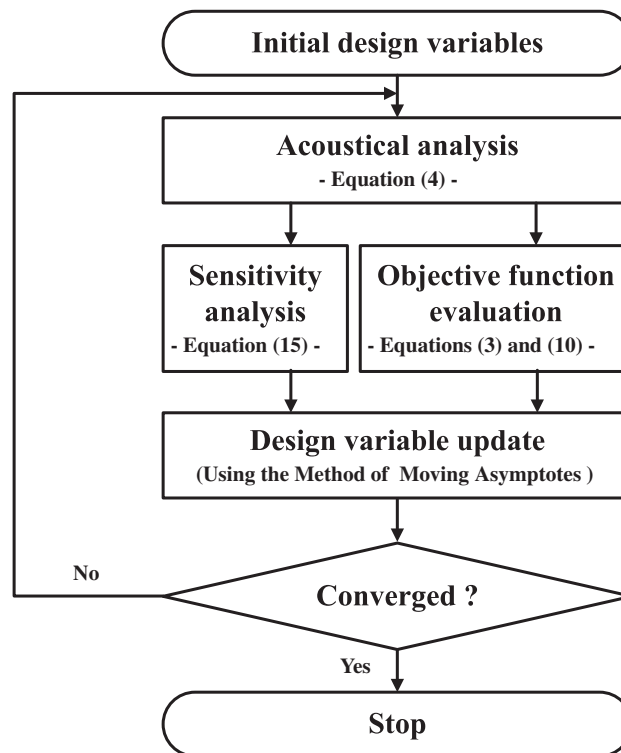


Figure 4. Flow chart of the topology optimization process used to solve the muffler design problem.

4. PARTITION LAYOUT OPTIMIZATION BY TOPOLOGY OPTIMIZATION METHOD

This section will present numerical results obtained by the topology optimization formulation given in Section 3. For future reference, the muffler shown in Figure 1(a) will be called the nominal muffler. Figure 4 shows the flow chart of the topology optimization process for solving the muffler design problem described above.

Recall that the TL of the nominal muffler becomes the largest at $f_1^{\max} = 173.2\text{ Hz}$, $f_2^{\max} = 519.6\text{ Hz}$, etc., and almost zero at the deep frequencies $f_1^{\min} = 346.4\text{ Hz}$, $f_2^{\min} = 692.9\text{ Hz}$. In the first case study (Case study I), four single target frequencies with a fixed total value of R_a will be considered. In Case study II, the effect of R_a on the optimal topological layouts of the expansion chamber muffler will be examined for the target frequency of $f_2^{\min} = 692.9\text{ Hz}$. In Case study III, the TL maximization problem involving multiple target frequencies will be studied. For all numerical

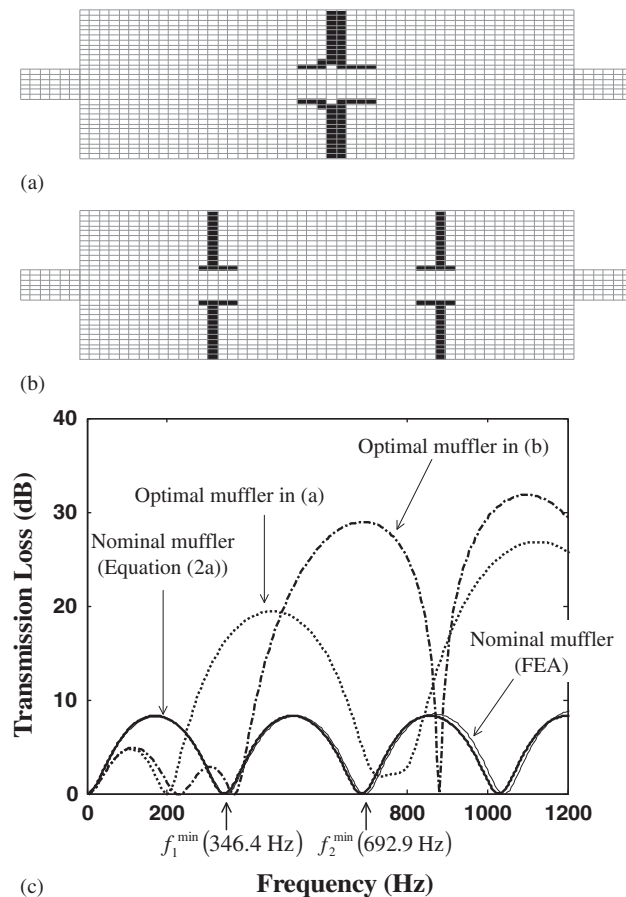


Figure 5. The transmission loss maximization at the deep frequencies of the nominal muffler in Figure 1: (a) optimized result for the TL maximization at $f_i = 346.4\text{ Hz}$; (b) optimized result for the TL maximization at $f_i = 692.9\text{ Hz}$; and (c) comparison of transmission loss curves.

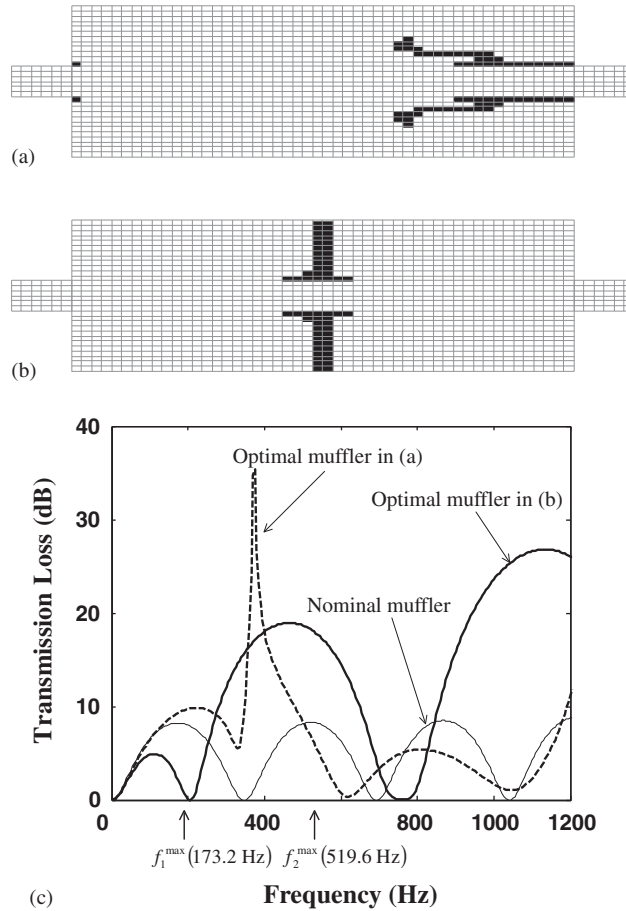


Figure 6. The transmission loss maximization at f_1^{\max} and f_2^{\max} of the nominal muffler in Figure 1: (a) optimized result for the TL maximization at $f_t=173.2\text{Hz}$; (b) optimized result for the TL maximization at $f_t=519.6\text{Hz}$; and (c) comparison of transmission loss curves.

simulations, the following acoustical properties of air at 20°C are used [20]:

$$\rho_{\text{air}} = 1.21 \text{ kg/m}^3, \quad c_{\text{air}} = 343 \text{ m/s}, \quad \rho_{\text{rigid}} = 10^7 \rho_{\text{air}}, \quad K_{\text{rigid}} = 10^9 K_{\text{air}}$$

The used geometries were determined on the basis of the work by Selamet and Ji [3]: $l=0.5 \text{ m}$, $d=0.15 \text{ m}$, $d_i=d_o=0.03 \text{ m}$, and $x_{12}=0.01 \text{ m}$. For all simulation results, the initial values of χ_r are set equal to zero. No filtering or post-processing is used in obtaining all the results in this work.

4.1. Case study I: Optimization at various single target frequencies

The acoustical topology optimization problem setup as Equations (10)–(13) is solved for two types of target frequencies. First, the deep frequencies f_1^{\min} and f_2^{\min} of the nominal muffler

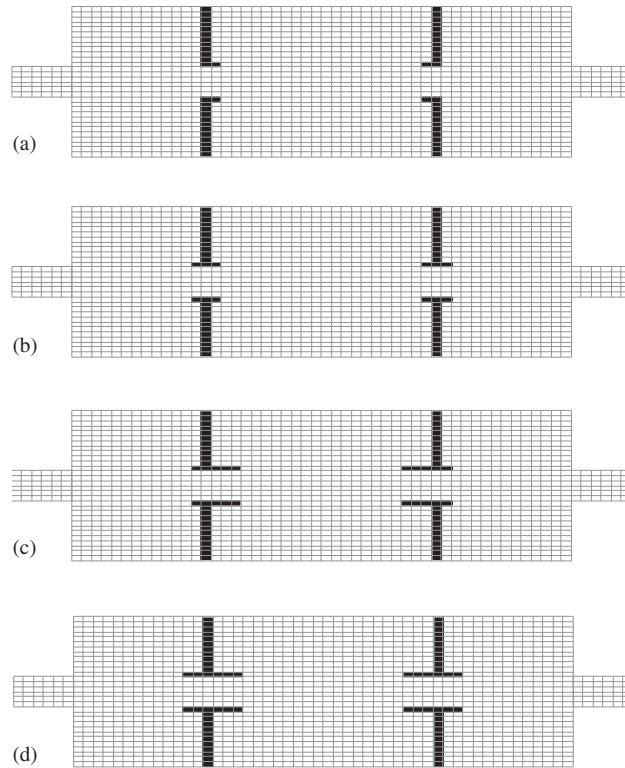


Figure 7. The effect of the number of allowed rigid body elements (R_a) on the optimized layout configuration. The target frequency is $f_2^{\min} = 692.9\text{Hz}$. The results are given for: (a) $R_a = 52$; (b) $R_a = 56$; (c) $R_a = 64$; and (d) $R_a = 68$.

(see Figure 1(b)) are chosen as target frequencies. Second, the target frequencies of f_1^{\max} and f_2^{\max} at which the nominal muffler has the maximal TL values are considered. Thus, the following four problems will be solved:

$$\text{Maximize TL}(f_1^{\min} = 346.4\text{Hz}) \tag{18a}$$

$$\text{Maximize TL}(f_2^{\min} = 692.9\text{Hz}) \tag{18b}$$

$$\text{Maximize TL}(f_1^{\max} = 173.2\text{Hz}) \tag{18c}$$

$$\text{Maximize TL}(f_2^{\max} = 519.6\text{Hz}) \tag{18d}$$

subject to

$$\sum_{r=1}^R \lambda_r / R \leq V_a = \frac{R_a}{R} = 0.05 \quad (V_a = 0.05: \text{equivalent to } R_a = 60) \tag{19}$$

Equation (19) states that the total number R_a of the allowed rigid body elements is fixed.

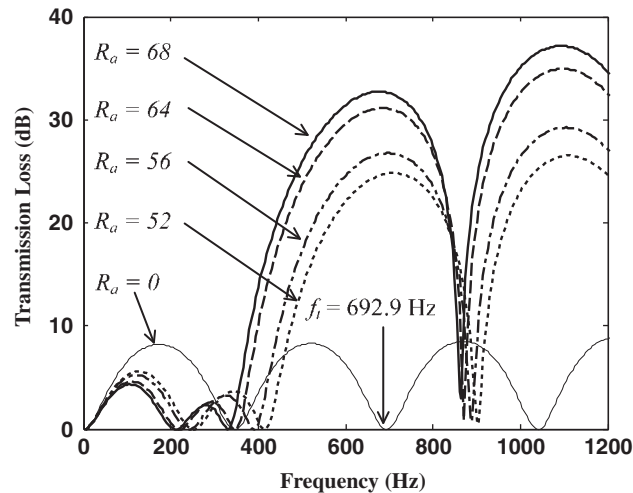


Figure 8. Comparison of the transmission loss for different expansion chamber configurations shown in Figure 7.

Figure 5 shows the optimized topological layouts and their TL curves obtained for the objective functions of Equations (18a) and (18b) and the constraint (19). The use of the optimized partition layouts in Figures 5(a) and (b) improved the TL values by 16.3 dB at f_1^{\min} and 28.9 dB at f_2^{\min} in comparison with the nominal muffler; see Figure 5(c). To check the validity of our finite element code, the calculated TL curve by the code is compared in Figure 5(c) with the exact result by Equation (2a). Except at relatively high frequencies, the two results are almost identical.

For the objective functions of Equations (18c) and (18d) and the constraint (19), the optimized results in Figure 6 are obtained. Figure 6(c) compares the TL values of the nominal muffler with those of the optimized mufflers (12.9% increase at f_1^{\max} and 120.6% increase at f_2^{\max}). The partition locations in Figures 6(a) and (b) are considerably different from those shown in Figures 5(a) and (b). It implies that optimized results strongly depend on a target frequency for a given R_a .

4.2. Case study II: The effect of the volume constraint

In general, the massive use of partitions is not desirable. Nevertheless, it is important to understand the effect of the rigid body element constraint, equivalently the partition volume constraint, on optimized results. For this study, Equations (18b) and (19) are solved for various values of R_a ranging from $R_a = 24$ to 84 with an increment of 4. Four representative optimized results corresponding to $R_a = 52, 56, 64$ and 68 are illustrated in Figure 7 and the corresponding TL curves in Figure 8.

The results in Figure 7 show that as R_a increases, the rigid body elements form a vertical partition in the first place and then a horizontal partition. It is noted that the location of the vertical partition corresponds very closely to the nodal line of the 2nd x -axial acoustic mode of the nominal muffler. Accordingly, the 2nd deep frequency of the optimized mufflers decreases as the TL value at the target frequency increases in Figure 8.

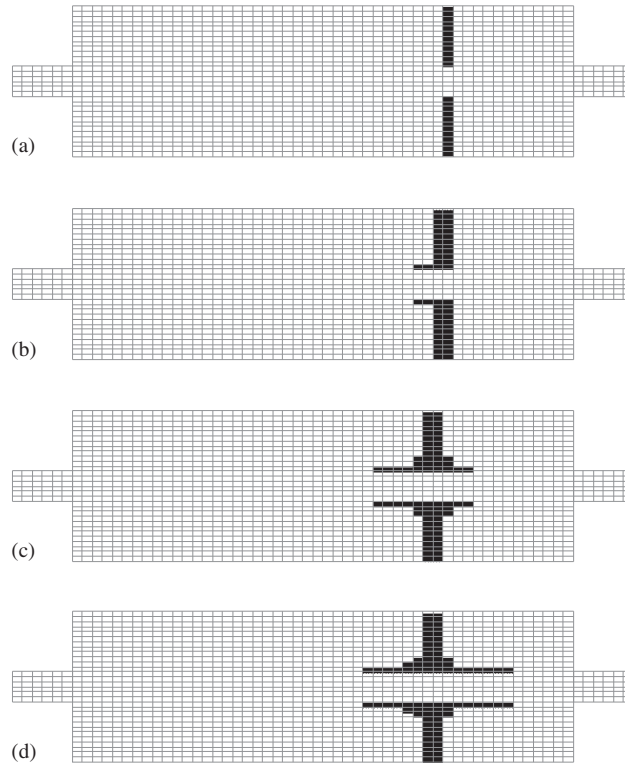


Figure 9. Simultaneous transmission loss maximization at 346.4 Hz (f_1^{\min} of a nominal muffler) and 692.9 Hz (f_2^{\min} of a nominal muffler). Different volume constraints were considered: (a) $R_a=24$; (b) $R_a=52$; (c) $R_a=72$; and (d) $R_a=84$.

4.3. Case study III: Simultaneous maximization at two deep frequencies

In this case study, the simultaneous TL maximization at two target frequencies is considered. The target frequencies are the two deep frequencies of the nominal muffler, in which case the objective function L in Equation (10) is

$$L = -[\text{TL}(f_1^{\min} = 346.4 \text{ Hz}) + \text{TL}(f_2^{\min} = 692.9 \text{ Hz})] \tag{20}$$

The optimized layouts for $R_a=24, 52, 72, 84$ are shown in Figure 9, and Figure 10 compares the corresponding TL curves with that of the nominal muffler. As R_a increases, TL values increase accordingly, especially at the target frequencies. An interesting point is that the TL values of optimized mufflers are not zero even at deep frequencies of all optimized mufflers; this phenomenon will be examined in the next section. Good solution convergence histories of TL values at the two target frequencies ($R_a=52$) are observed from Figure 11.

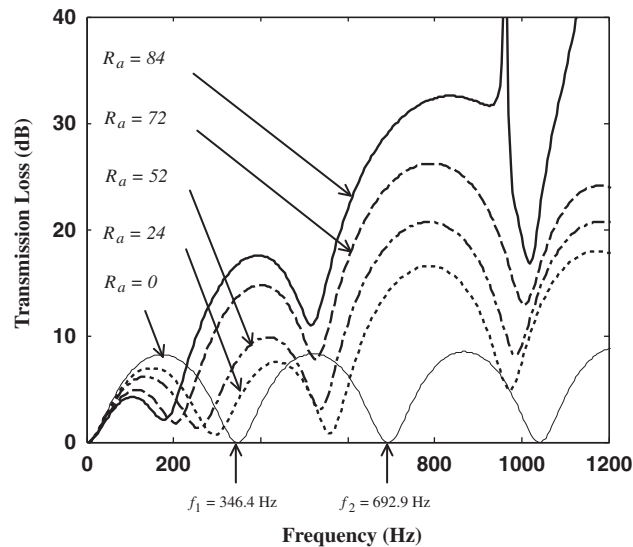


Figure 10. Transmission loss curves for the optimized topological layouts shown in Figure 9.

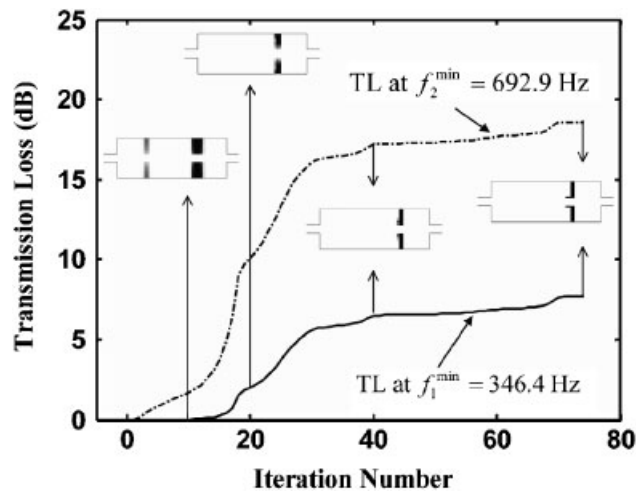


Figure 11. The optimization history for simultaneous transmission loss maximization for $f_1^{\min} = 346.4$ and $f_2^{\min} = 692.9$ Hz (the value of $R_a = 52$ was used).

5. DISCUSSION

5.1. Acoustical properties of a rigid body

As far as the acoustical properties of a rigid body are considered, one can show that if the characteristic impedance of an acoustical material is sufficiently high, the material can accurately

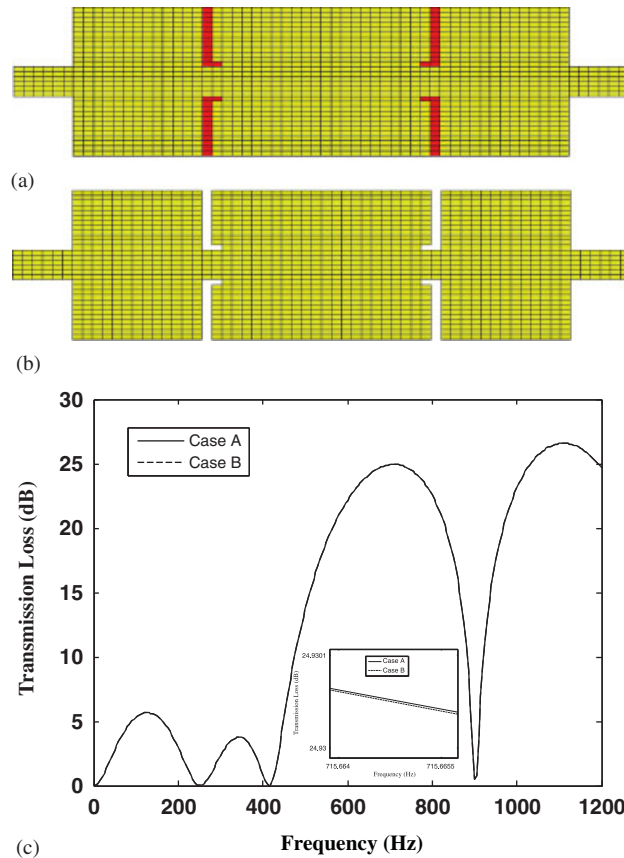


Figure 12. Test problem to check transmission characteristics of a rigid body: (a) Case A: the optimized layout in Figure 7(a) having the simulated rigid-wall elements (=rigid body elements, in dark shaded area) with $\rho_{\text{rigid}} = 10^7 \rho_{\text{air}}$ and $K_{\text{rigid}} = 10^9 K_{\text{air}}$; (b) Case B: the optimized layout in Figure 7(a) having the true rigid-wall condition; and (c) transmission loss curve comparison.

model the acoustic property of a rigid wall, i.e. it can reflect an incident acoustic wave almost completely. The reason for taking a large value instead of using the exact condition is to facilitate the overall optimization process; without this technique, it is not possible to use an efficient gradient-based optimizer. To check the validity of the values of the acoustical properties used in this paper, we compared in Figure 12 the transmission loss curves of the optimized layout in Figure 7(a) with the simulated rigid wall elements (=rigid body elements) with ($\rho_{\text{rigid}} = 10^7 \rho_{\text{air}}$ and $K_{\text{rigid}} = 10^9 K_{\text{air}}$) (Case A) and the equivalent layout with the exact rigid-wall boundary condition (Case B). While the dark shaded area in Figure 12(a) is filled with the rigid body of $\rho_{\text{rigid}} = 10^7 \rho_{\text{air}}$ and $K_{\text{rigid}} = 10^9 K_{\text{air}}$, acoustic elements in Figure 12(b) are not assigned to the same area for imposing exact rigid-wall boundary condition to the outline of the partitions. The acoustical analysis was carried out by using commercial finite element package, Sysnoise 5.5. Figure 12(c) shows that there is little difference between the two TL curves of two cases. It means that the values of $\rho_{\text{rigid}} = 10^7 \rho_{\text{air}}$ and $K_{\text{rigid}} = 10^9 K_{\text{air}}$ are valid so that a rigid body could simulate rigid wall.

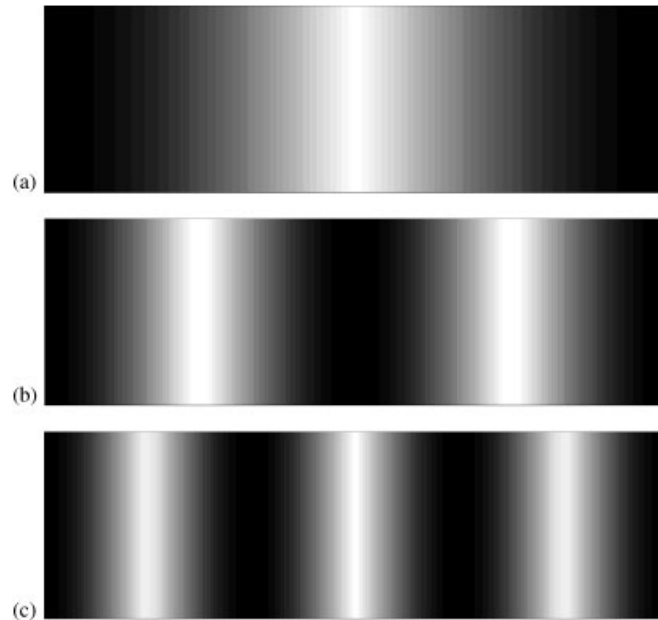


Figure 13. (a) The first acoustic mode (1,0); (b) second acoustic mode (2,0); and (c) third acoustic mode (3,0) of the nominal muffler.

5.2. Physical interpretation of optimized results

This section is devoted to the physical interpretation of the optimized results in the previous section. To understand the acoustical characteristics of the optimized muffler, acoustical eigenmodes and eigenfrequencies of the optimized mufflers obtained in Case studies II and III and those of the nominal muffler are compared. Since the effect of inlet and outlet regions on the acoustical characteristics of a muffler is marginal, the acoustical eigenvalue analysis is performed for the expansion chambers surrounded by rigid-wall boundaries. This will simplify the analysis.

Figure 13 shows the first three x -axial acoustic modes of the nominal muffler. The eigenfrequencies of the acoustic modes almost coincide with the deep frequencies indicated in Figure 1(b). The gray line in Figure 13 corresponds to the absolute value of the normalized acoustic pressure. Each of a white vertical line in the acoustic modes represents a nodal line. The presence of a higher acoustic pressure level in the left and right ends implies that even a small input pressure pulsation in one side around the eigenfrequencies can be easily transmitted to the other side. This means that the nominal muffler should not be used around those frequencies.

Figure 14(a) shows how the eigenfrequencies of optimized mufflers vary in Case study II as R_a increases. One can see that the optimization is conducted so as to locate the target frequency between the two deep frequencies of the optimized mufflers because local maxima of the TL values occur somewhere between the consecutive deep frequencies.

By examining Figure 8, an interesting observation can be made: the TLs of the optimized mufflers are almost zero at their second deep frequency while they are not at their third deep frequency. The reason is revealed by examining the 2nd and 3rd acoustic modes of the optimized muffler with $R_a = 68$ (see Figure 7(d)). The acoustic pressures at both ends are very high for the

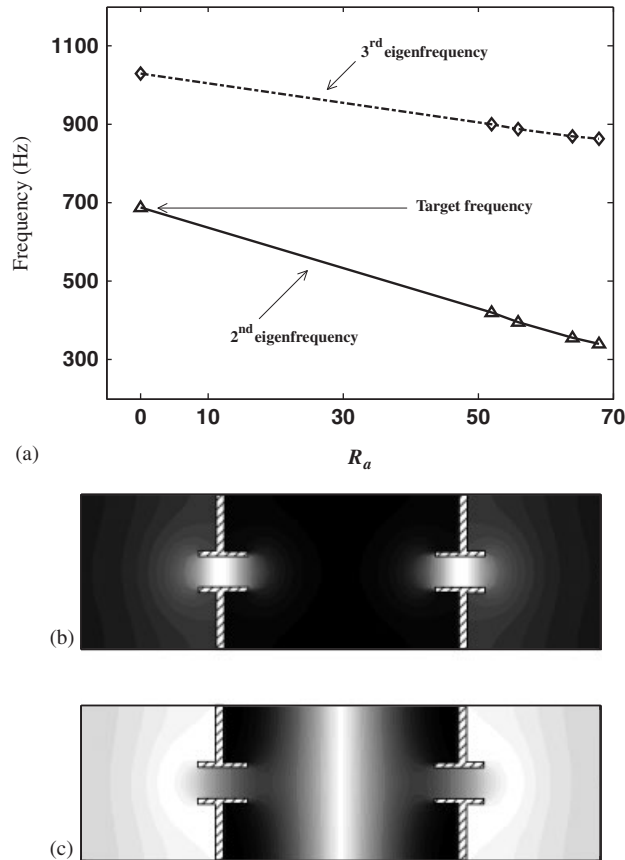


Figure 14. Acoustical characteristics of optimized mufflers in Case study II: (a) change in the 2nd and 3rd eigenfrequencies of the optimized mufflers with the number of rigid body elements; (b) the 2nd acoustic mode of the optimized muffler in Figure 7(d); and (c) the 3rd acoustic mode of the optimized muffler in Figure 7(d).

2nd acoustic mode in Figure 14(b), while they are relatively low for the 3rd acoustic mode in Figure 14(c). This means that input pressure pulsation in one side at a frequency around the third eigenfrequency cannot excite the third acoustic mode as much as input pressure pulsation at a frequency around the second eigenfrequency excites the second acoustic mode. Therefore, the TL around the 3rd deep frequency of the optimized muffler has a non-vanishing value.

The validity of the above-mentioned argument can be also confirmed by a close examination of the acoustic modes and eigenfrequencies of the optimized mufflers obtained in Case study III. Figure 15 shows how the eigenfrequencies of the muffler vary with R_a . By the optimization, the deep frequencies of the optimized muffler move away from the target frequencies, which are the deep frequencies of the nominal muffler. Again, the acoustic modes of the optimized muffler for $R_a=72$ are plotted in Figure 16. The acoustic pressure in one side is relatively low for the 1st, 2nd and 4th acoustic modes, whose eigenfrequencies closely coincide with the 1st, 2nd and 3rd deep frequencies of the optimal mufflers in Figure 9(c). Therefore, input pressure fluctuation at

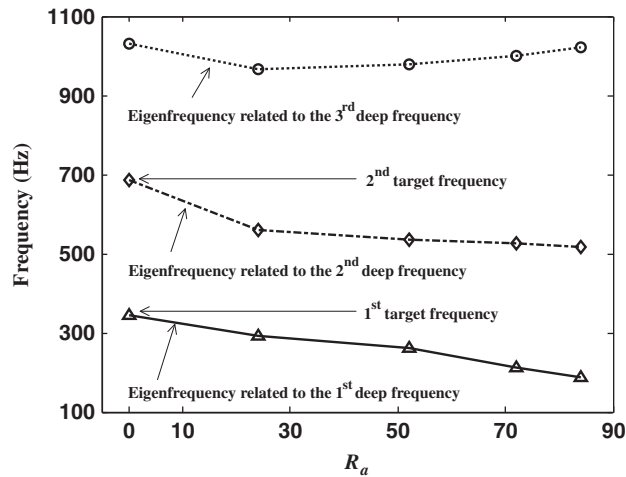


Figure 15. Change in eigenfrequencies of the optimized topologies, related to deep frequencies, with the number of rigid body elements.

an inlet cannot be transmitted to the outlet at frequencies around the eigenfrequencies well. Since the acoustic pressure of the 3rd acoustic mode has the minimum values in both sides as shown in Figure 16(c), no deep frequency exists near the eigenfrequency.

It will be interesting to compare the acoustical attenuation performances of an optimized muffler by the topology optimization and a muffler, which may be designed by conventional design practice [3]. The conventional practice is to adjust the length l_1 of the extended inlet for increasing a TL value at a target frequency, which is $f_t = 692.9$ Hz in this comparison. A muffler designed by the practice is illustrated in Figure 17(a). The optimized value of l_1 is $l_1 = 0.11$ m. The optimized muffler with $R_a = 84$ obtained by the topology optimization is also shown in Figure 17(b). The TL curves of the two mufflers in Figures 17(a) and (b) are compared in Figure 18 with that of the nominal muffler. The TL values of the two mufflers in Figures 17(a) and (b) increased at the target frequency, but the overall behavior of the TL curves is quite different from each other. The TL values of the muffler of Figure 17(a) increased at the target frequency without decreasing at 'all' other frequencies and a peak value existed around the target frequency. On the contrary, the TL values of the optimized muffler in Figure 17(b) were decreased at other frequencies. By sacrificing the TL values at other frequencies, the TL values around the target frequency in the muffler of Figure 17(b) were maximized. That is, the TL level at the effective frequency range of the muffler optimized by the present approach is much higher than that of the muffler designed by the conventional design method; the relative difference is about 10 dB.

5.3. Mesh dependence

In this section, the effects of mesh sizes and shapes on the optimized results will be investigated numerically. For this investigation, three finite element models of the muffler in Figure 1(a) having different mesh sizes are considered, while the same volume constraint is used. Specifically, the

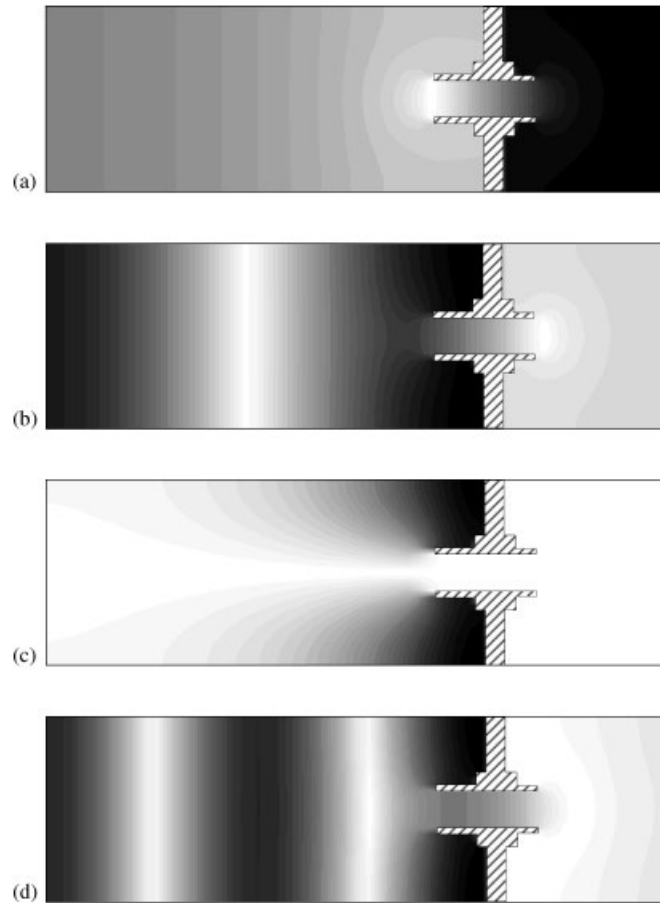


Figure 16. (a) The first acoustic mode; (b) second acoustic mode; (c) third acoustic mode; and (d) fourth acoustic mode of the optimized muffler of Figure 9(c).

following three meshes are used:

Mesh A: $\Delta x = 0.01$ m, $\Delta y = 0.005$ m, $N_e = 1500$, $R = 1200$

Mesh B: $\Delta x = 0.02$ m, $\Delta y = 0.005$ m, $N_e = 750$, $R = 600$

Mesh C: $\Delta x = 0.01$ m, $\Delta y = 0.01$ m, $N_e = 750$, $R = 600$

where Δx and Δy denote the uniformly spaced element sizes along the x -direction and the y -direction, respectively, and N_e is the number of total elements in the expansion chamber.

Figure 19 compares three optimized results for $f_t = 346.4$ Hz and $V_a = \frac{1}{50}$ and the corresponding TL curves. As shown in Figures 19(a) and (c), the optimized mufflers obtained by using Mesh A and Mesh C have the same optimal topology and TL at the target frequency ($TL_{(f=f_t)} = 8.1$ dB). However, the optimal topology obtained by using Mesh B (Figure 19(b)) has a lower TL value ($TL_{(f=f_t)} = 1.1$ dB). The coincidence in the TL values by Mesh A and Mesh C is due to the fact that the optimized topologies in Figures 19(a) and (c) turn out to have the same length of the vertical partitions because Mesh A and Mesh C have the same Δx . Thus, one can see apparent

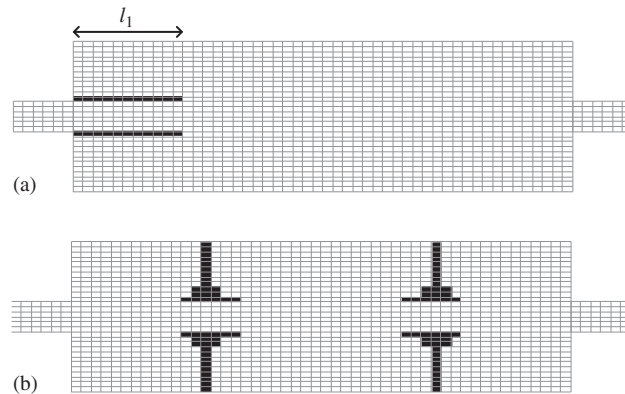


Figure 17. Layouts of two optimized mufflers designed for the target frequency of 692.9 Hz: (a) by a conventional method and (b) by the topology optimization method ($R_a = 84$).

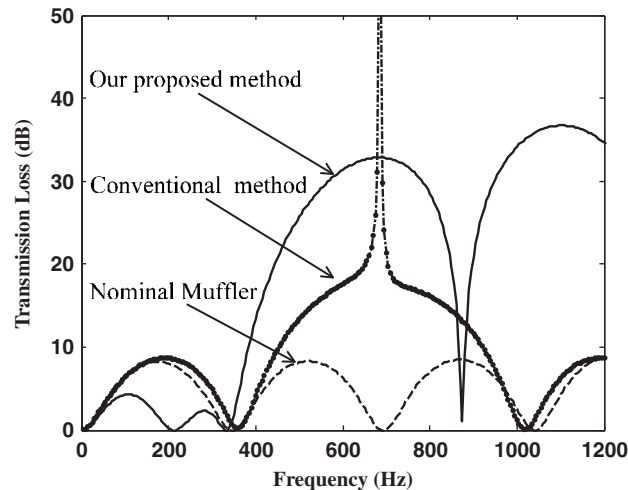


Figure 18. The comparison of the transmission loss curves of the nominal muffler and the optimized muffler shown in Figures 17(a) and (b).

effects of mesh on the solutions from Figure 19, but the same topological layout at the same location was obtained for the three different finite element models.

Figure 20 compares three optimized topologies and the corresponding TL curves by using the same meshes as used for Figure 19 but a different volume ratio of $V_a = \frac{17}{300}$ ($f_t = 346.4$ Hz). As shown in Figure 20, the optimized partition layouts are not exactly the same but they have the same topologies. Also, the main vertical partitions are located at the same x coordinate for the meshes used.

As in other structural problems, the mesh dependence is apparent in this problem. To control mesh dependence, one may consider employing the perimeter control of a mechanical element, restricting gradients, filtering the sensitivities and others (see, e.g. [21]). Nevertheless, the solutions

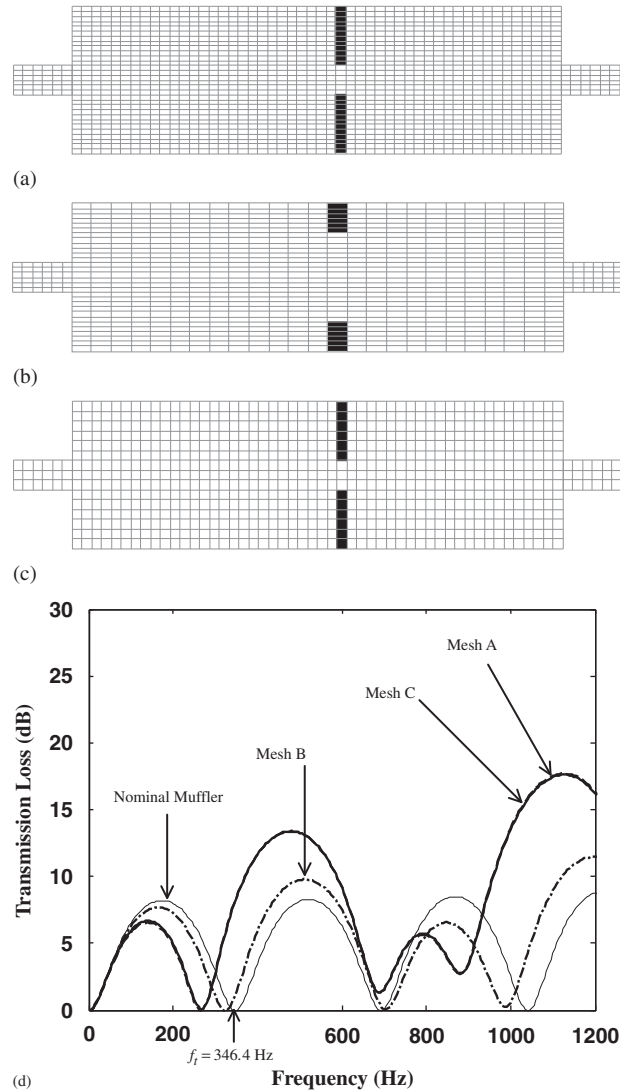


Figure 19. Optimized results obtained by using three different finite element models for $f_t = 346.4$ Hz and $V_a = \frac{1}{50}$: (a) Mesh A; (b) Mesh B; (c) Mesh C; and (d) the corresponding transmission loss curves.

by using different meshes give relatively consistent results—the locations of vertical partitions and topologies are almost identical or not much different from each other.

6. CONCLUDING REMARKS

In this investigation, acoustical topology optimization was formulated to maximize the TL of a concentric expansion chamber muffler at target frequencies. With the formulation, non-traditional

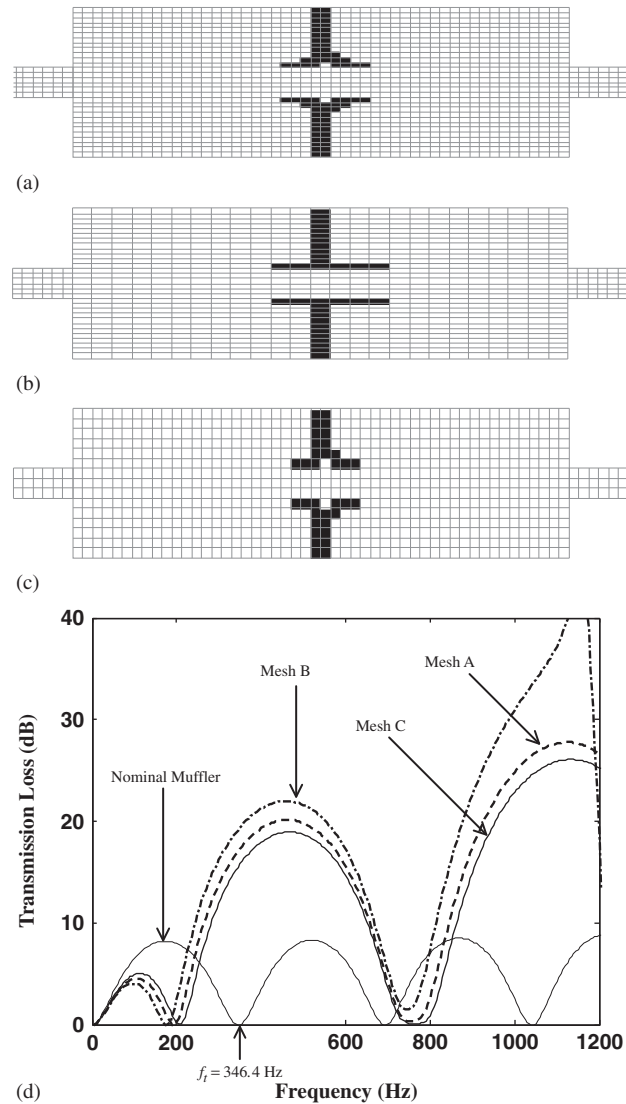


Figure 20. Optimized results obtained by using three different finite element models for $f_t = 346.4$ Hz and $V_a = \frac{17}{300}$: (a) Mesh A; (b) Mesh B; (c) Mesh C; and (d) the corresponding transmission loss curves.

partition layouts yielding much higher TL values were obtained. A special emphasis was put on the physical interpretation of the partition layouts, especially for the non-conventional optimized mufflers. Among others, higher TL values for the optimized layouts at the target frequencies result from the sacrifice of the TL at other frequencies. Although the global optimal solutions were not guaranteed because a gradient-based optimizer was employed, the obtained results successfully improved the TL values for all problems considered. Whether the target frequencies were the deep frequencies of the nominal muffler or not, the TL values of the optimized muffler by the

developed method always increased. The underlying result and method are expected to be utilized for optimizing three-dimensional non-concentric expansion chamber mufflers as well as cylindrical symmetric mufflers. If flow analysis for mufflers is also considered in the future, the impact of the subsequent topology optimization in muffler design can be significant.

ACKNOWLEDGEMENTS

This research was supported by the National Creative Research Initiatives Program (Korea Science and Technology Foundation Grant Nos. 2007-019 and 0420-2008-0011) contracted through the Institute of Advanced Machinery and Design at Seoul National University.

REFERENCES

- Selamet A, Radavich PM. The effect of length on the acoustic attenuation performance of concentric expansion chambers: an analytical, computational and experimental investigation. *Journal of Sound and Vibration* 1997; **201**:407–426.
- Åbom M. Derivation of four-pole parameters including higher order mode effects for expansion chamber mufflers with extended inlet and outlet. *Journal of Sound and Vibration* 1990; **137**(3):403–418.
- Selamet A, Ji ZL. Acoustic attenuation performance of circular expansion chambers with extended inlet/outlet. *Journal of Sound and Vibration* 1999; **223**(2):197–212.
- Selamet A, Denia FD, Besa AJ. Acoustic behavior of circular dual-chamber mufflers. *Journal of Sound and Vibration* 2003; **265**:967–985.
- Panigrahi SN, Munjal ML. Plane wave propagation in generalized multiply connected acoustic filters. *Journal of the Acoustical Society of America* 2005; **118**(5):2860–2868.
- Selamet A, Ji ZL. Acoustic attenuation performance of circular flow-reversing chambers. *Journal of the Acoustical Society of America* 1998; **104**(5):2867–2877.
- Yeh L, Chang Y, Chiu M. Numerical studies on constrained venting system with reactive mufflers by GA optimization. *International Journal for Numerical Methods in Engineering* 2006; **65**:1165–1185.
- Chang Y, Chiu M. Shape optimization of one-chamber perforated plug/non-plug mufflers by simulated annealing method. *International Journal for Numerical Methods in Engineering* 2008; **74**:1592–1620.
- Chang Y, Yeh L, Chiu M. Optimization of double-layer absorbers on constrained sound absorption system by using genetic algorithm. *International Journal for Numerical Methods in Engineering* 2005; **62**:317–333.
- Seo S, Kim Y. Silencer design by using array resonators for low-frequency band noise reduction. *Journal of the Acoustical Society of America* 2005; **118**(4):2332–2338.
- Barbieri R, Barbieri N. Finite element acoustic simulation based shape optimization of a muffler. *Applied Acoustics* 2006; **67**(4):346–357.
- Lee J, Wang S, Dikec A. Topology optimization for the radiation and scattering of sound from thin-body using genetic algorithms. *Journal of Sound and Vibration* 2004; **276**:899–918.
- Wadbro E, Berggren M. Topology optimization of an acoustic horn. *Computer Methods in Applied Mechanics and Engineering* 2006; **196**:420–436.
- Dühning MB, Jensen JS, Sigmund O. Acoustic design by topology optimization. *Journal of Sound and Vibration* 2008; **317**:557–575.
- Wu TW, Wan GC. Muffler performance studies using a direct mixed-body boundary element method and a three-point method for evaluating transmission loss. *ASME Journal of Vibration and Acoustics* 1996; **118**:479–484.
- Svanberg K. The method of moving asymptotes: a new model for structural optimization. *International Journal for Numerical Methods in Engineering* 1987; **24**(2):359–373.
- Jensen JS, Sigmund O. Systematic design of acoustic devices by topology optimization. *Proceeding of the 12th International Congress on Sound and Vibration*, Lisbon, Portugal, 2005.
- Morse PM, Ingard KU. *Theoretical Acoustics*. McGraw-Hill Book Company: New York, 1986.
- Munjal ML. *Acoustics of Ducts and Mufflers with Application to Exhaust and Ventilation System Design*. Wiley: New York, 1987.
- Kinsler LE, Frey AR, Coppens AB, Sanders JV. *Fundamentals of Acoustics*. Wiley: New York, 1982.
- Bendsøe MP, Sigmund O. *Topology Optimization—Theory, Methods and Applications*. Springer: New York, 2004.